OATAO

Open Archive Toulouse Archive Ouverte

Open Archive Toulouse Archive Ouverte (OATAO)

OATAO is an open access repository that collects the work of Toulouse researchers and makes it freely available over the web where possible

This is an author's version published in: **http://oatao.univ-toulouse.fr/25464**

Synergistic effect between 8-hydroxyquinoline and benzotriazole for the corrosion protection of 2024 aluminium alloy: A local electrochemical impedance approach

Sabrina Marcelin, Nadine Pébère *

Université de Toulouse, CIRIMAT, UPS/INPT/CNRS, ENSIACET, 4, Allée Emile Monso, CS 44362, 31030 Toulouse cedex 4, France

ARTICLE INFO

ABSTRACT

This work is devoted to the corrosion inhibition of the 2024 aluminium alloy (AA2024) in neutral aqueous solution by 8-hydroxyquinoline (8-HQ) and benzotriazole (BTA). First, current-voltage curves and global electrochemical impedance measurements confirmed that 8-HQ and BTA are two effective corrosion inhibitors for AA2024. Mixing the two compounds led to a synergistic effect for the corrosion protection of the alloy. From the impedance data analysis, it was shown that 8-HQ acted mainly on the aluminium matrix with an additional action of the BTA on the intermetallic particles. Then, to analyse the role of the inhibitors on the galvanic coupling between the aluminium matrix and the particles, local electrochemical impedance measurements were performed on a model system (Al/Cu couple). It was shown that in the presence of 8-HQ or BTA alone, the galvanic coupling between copper and aluminium was little reduced while in the presence of both compounds together it was strongly limited. The local impedance results confirmed the specific inhibition of the 8-HQ and of the BTA on Al and Cu respectively.

1. Introduction

Among the numerous studies concerning the replacement of Cr(VI) for the corrosion protection of structural alloys, such as the 2XXX series, some compounds, such as rare earth salts (mostly cerium) [1–9] or organic compounds, such as triazole, thiazole derivatives and more recently carbamate derivatives [10–16], have presented interesting corrosion protection activity. It was shown that this type of inhibitor acts on the copper-rich particles decreasing their cathodic activity. Despite their promising performance, these compounds do not achieve the same level of protection as chromates. To increase corrosion protection, the use of mixtures of inhibitors could be a good strategy. Recently, multifunctional inhibitors, offering both anodic and cathodic inhibition, were investigated: inorganic cations (rare earths) acting on the cathodic sites and organic anions, acting on the anodic sites [17–20].

Among the organic compounds, 8-hydroxyquinoline (8-HQ) and benzotriazole (BTA) were studied as corrosion inhibitors in aqueous solution [10–12] or encapsulated in reservoirs and added to organic or sol–gel coatings for the corrosion protection of AA2024 [21,22]. 8-HQ is known for its chelating properties on different metals [10–12,23,24] and BTA is well known as a corrosion inhibitor for copper [25]. These compounds are generally studied separately.

The aim of the present work is to investigate the 8-HQ + BTA mixture for the corrosion protection of 2024 aluminium alloy and more particularly to obtain a clearer picture of the inhibitive effect of each compound. The final goal of this study is to develop a methodology which could be used to evaluate and compare the efficiency of different compounds or inhibitive mixtures. The methodology chosen is based on the use of both conventional and local electrochemical impedance spectroscopy (EIS). It is important to keep in mind that the degradation of the AA2024 is mainly due to local galvanic coupling between the intermetallic particles and the surrounding matrix [26–33]. To investigate the action of the inhibitor molecules on the particles, an Al/Cu model couple was used. In a previous study, this model couple was designed to understand the corrosion phenomena associated with copper-rich intermetallics in aluminium alloys [34] and was recently used to study the corrosion inhibition of AA2024 by sodium decanoate [14].

2. Experimental procedure

The materials and the electrochemical techniques used are presented in this section. The AA2024 electrode surface was examined

* Corresponding author. Fax: +33 5 34 32 34 99.
E-mail address: Nadine.Pebere@ensiacet.fr (N. Pébère).

by optical and scanning electron microscopy after being immersed in the solution containing the inhibitors.

2.1. Materials

8-hydroxyquinoline (8-HQ) and benzotriazole (BTA) were analytical grade reagents (purity = 99%) from Alfa Aesar and Sigma–Aldrich respectively, and were used as received. The concentrations of 8-HQ (3×10^{-3} M) or for BTA (10^{-2} M) were chosen near their solubility limits in neutral solution. These concentrations allowed the highest efficiency of the compounds tested alone to be obtained.

For the conventional electrochemical measurements, the corrosive medium was prepared from deionised water by adding 0.1 M Na_2SO_4 and a small concentration of chloride (0.05 M NaCl) (reagent grade). Sodium sulphate was chosen to increase the conductivity of the solution and for its low corrosiveness toward aluminium alloys. For the local impedance experiments (Al/Cu model couple), dilute solutions were used: 10^{-3} M NaCl, 10^{-2} M BTA, 3×10^{-3} M 8-HQ or 10^{-2} M BTA + 3×10^{-3} M 8-HQ. The inhibitors were tested without NaCl in the deionised water to keep a solution with a low conductivity [34]. The electrolytes were in contact with air at room temperature ($20\,°C \pm 2\,°C$).

Aluminium alloy 2024 T351 was used for the investigations. The average chemical composition of the alloy is given in Table 1. Electrochemical experiments were carried out on an AA2024 T351 rod of 1 cm^2 cross-sectional area machined from a rolled plate (cylinder surface parallel to the plane of rolling). For comparison, some electrochemical tests were performed on pure aluminium (99.9999 wt.%), kindly provided by Praxair or on pure copper (99.9 wt.%) purchased from Alfa Aesar. The body of the rods (1 cm^2 cross-sectional area) was covered with a heat-shrinkable sheath, leaving only the tip of the rod in contact with the solution. The samples were abraded with successive SiC papers and diamond pastes (grade 1200–1 μm), cleaned in ethanol in an ultrasonic bath and finally dried in warm air.

In order to study the interactions between the inhibitors and the matrix and/or the intermetallic particles, a simple system consisting of a pure aluminium/pure copper (Al/Cu) couple was used [34]. The electrode was prepared as follows: a cylinder of pure aluminium (99.9999 wt.%) was drilled in its centre and a cylinder of pure copper (99.9 wt.%) was introduced by force into the hole (Fig. 1). The radii were 1 and 0.315 cm for the aluminium and copper bars, respectively. The assembly of the two materials gave a perfectly joined interface, avoiding crevice corrosion due to surface defects. The electrical resistance between Cu and Al was lower than 0.5 Ω. The electrode was then embedded in an epoxy resin. Before immersion in the electrolyte, the Al/Cu disk electrode was prepared in the same way as the AA2024 or pure Al and Cu rods.

2.2. Electrochemical measurements

For the conventional experiments, a three-electrode cell was used with a platinum grid auxiliary electrode, a saturated calomel reference electrode (SCE) and the rod of AA2024 or the pure Al rod as rotating disk electrode. The rotation rate was fixed at 500 rpm. Polarisation curves and electrochemical impedance measurements were obtained using a Biologic VSP apparatus. The anodic and the cathodic parts were obtained independently from the corrosion potential at a potential sweep rate of 0.6 V/h. Impedance

diagrams were obtained at the corrosion potential over a frequency range of 65 kHz to a few mHz with eight points per decade using a 20 mV peak-to-peak sinusoidal potential. The electrochemical results were obtained from at least three experiments to ensure reproducibility.

The corrosion behaviour of the model couple with and without inhibitor was studied by local electrochemical impedance spectroscopy (LEIS). The measurements were carried out with a Solartron 1287 Electrochemical Interface, a Solartron 1250 frequency response analyser and a Scanning Electrochemical Workstation Model 370 (Uniscan Instruments). This method used a five-electrode configuration. Details are provided elsewhere [35–39]. The probe (i.e., a bi-electrode allowing local current density measurement) was stepped across a selected area of the sample. The analysed part had an area of 14 mm × 14 mm and the step size was 400 μm in the X and Y directions. Maps were obtained at a fixed frequency, chosen in the present case at 10 Hz, and admittance was plotted rather than impedance to improve the visualization of the result. Local impedance diagrams were recorded over a frequency range of 3 kHz–300 mHz with ten points per decade. The time to record all the local diagrams (from the centre to the edge) was lower than 60 min. The local impedance measurements were carried out in a low conductivity medium to optimize resolution. The measured conductivities of the different media are reported in Table 2. With the experimental set up used, only the normal component of the current was measured.

2.3. Surface characterization

The AA2024 surface was observed after 20 h of immersion in the solution (0.1 M Na_2SO_4 + 0.05 M NaCl) containing the inhibitors by a scanning electron microscope with a Leo 435VP apparatus to obtain a better description of the corrosion morphology, particularly on the intermetallic particles. Observations of the Al/Cu interface of the model couple were also performed by optical microscopy with a Nikon Eclipse MA200 microscope after 20 h of immersion in the solution containing the inhibitors.

3. Results and discussion

Fig. 2 illustrates the variation of the free corrosion potential (E_{corr}) of the AA2024 in a 0.1 M Na_2SO_4 + 0.05 M NaCl solution without inhibitor or in the presence of inhibitors: 8-HQ, BTA or a mixture of the two compounds. Without inhibitor, E_{corr} stabilizes rapidly whereas in the presence of the inhibitors E_{corr} increases with time
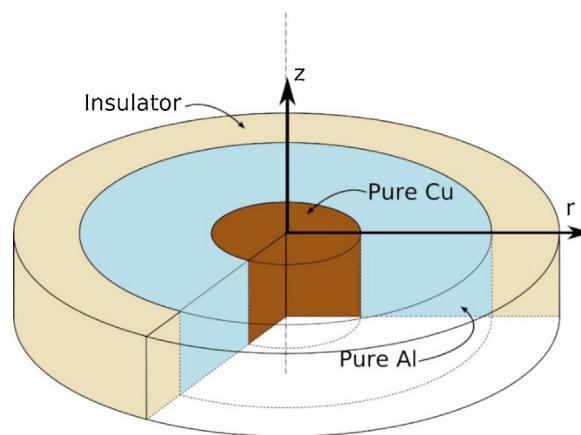

Fig. 1. Schematic representation of the pure aluminium/pure copper model couple. The radii of the two cylinders were equal to 1 and 0.315 cm for aluminium and copper bars, respectively. The electrode was then embedded in an epoxy resin so that a disk electrode was obtained at the extremity.

Table 2
Electrolyte conductivity with and without inhibitors in deionised water.

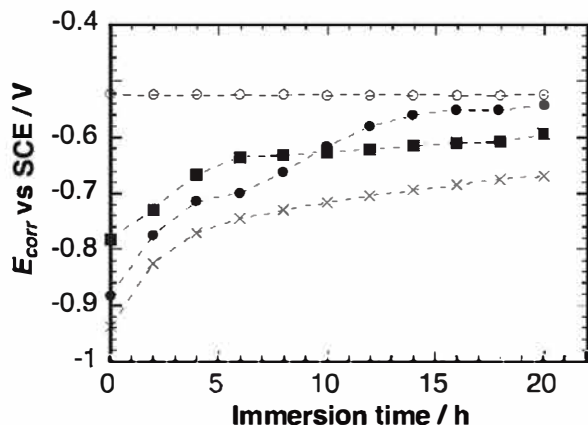|	10^{-3} M NaCl	8-HQ (3×10^{-3} M)	BTA (10^{-2} M)	8-HQ (3×10^{-3} M) + BTA (10^{-2} M)
Conductivity (μS cm^{-1})	101.5	2.1	2.1	6.5

Fig. 2. Corrosion potential (E_{corr}) of AA2024 as a function of time in a 0.1 M Na$_2$SO$_4$ + 0.05 M NaCl solution: (○) without inhibitor; (■) with BTA; (●) with 8-HQ and (×) with 8-HQ + BTA; electrode rotation rate: 500 rpm.

and then it stabilizes at approximatively 20 h. This immersion time corresponds to a stationary state and allows the compounds' efficiency to be compared. Thus, in the present study, all the electrochemical results and surface observations are shown after 20 h of immersion.

3.1. Polarisation curves

Fig. 3 shows the polarisation curves obtained for the AA2024 in the solution containing 8-HQ or BTA or a mixture of the two compounds. The curve without inhibitor is also reported for comparison. In the presence of BTA, the cathodic curve presents a region of mixed kinetic control of oxygen reduction. On the cathodic plateau, the current density is ten times lower than in the absence of inhibitor. In the presence of 8-HQ, the length of the cathodic plateau is reduced and, below −0.85 V/SCE, a rapid raise of the cur-
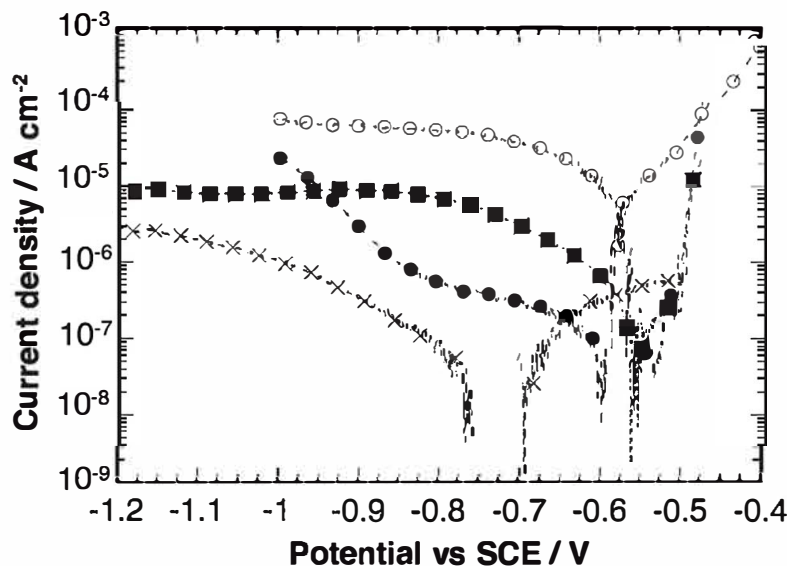
rent is observed. On the plateau, the current densities are lower than those measured in the presence of BTA. In the presence of the mixture of the two compounds, there is a significant drop of the cathodic current densities. Close to the corrosion potential (E_{corr}), within a potential range of 200 mV, the current densities remain low (<1 μA cm^{-2}) compared to the values measured in the absence of inhibitor (>100 μAcm^{-2}). In the anodic range, near E_{corr}, the polarisation curves obtained with the BTA or with the 8-HQ show a slight decrease of the current densities. At more positive potentials (around −0.5 V/SCE), an abrupt increase of the current densities due to the breakdown of the passive film and to the development of pits is observed (E_{pit} = −0.5 V/SCE). In the presence of the mixture, E_{corr} is shifted in the cathodic direction and an anodic current plateau can be seen. Then, around −0.5 V/SCE, an increase of the current is observed, as in the presence of 8-HQ or BTA. Under spontaneous corrosion conditions, pits will nucleate if $E_{corr} \geq E_{pit}$. Without inhibitor, $E_{corr} = E_{pit}$ and in the presence of the inhibitive mixture, E_{corr} is shifted in the cathodic direction. Therefore, the probability that the development of pits occurs decreases.

Ex situ observations of the electrode surface were performed by SEM after 20 h of immersion in the electrolyte containing each inhibitor or the inhibitor mixture. SEM micrographs of the intermetallic particles are reported in Fig. 4. In the presence of BTA, most of the particles are attacked (Fig. 4a and b). A deep crevice was formed at the matrix/particle interface. The crevice is partially related to the dissolution of the Al matrix close to the interface [34]. In the presence of 8-HQ, mainly the Al$_2$CuMg particles were attacked (Fig. 4c) and most of the others remained undamaged (Fig. 4d). In the presence of the mixture, neither the observed particles (Fig. 4e and f) nor the matrix were corroded.

The results obtained from the polarisation curves were confirmed by the SEM observations and accounted for a synergistic effect between 8-HQ and BTA for the corrosion protection of AA2024. SEM micrographs showed that in the presence of BTA or 8-HQ alone, the corrosion processes associated with the galvanic coupling between the particles and the matrix remained active
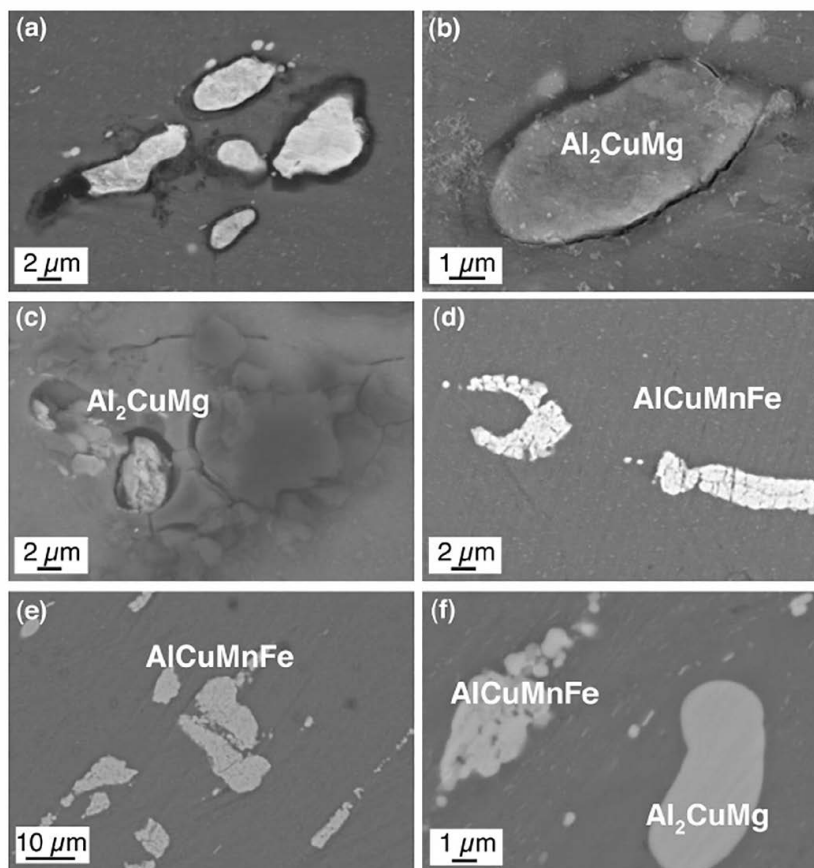

Fig. 3. Polarization curves obtained on AA2024 after 20 h of immersion in a 0.1 M Na$_2$SO$_4$ + 0.05 M NaCl solution: (○) without inhibitor; (■) with BTA; (●) with 8-HQ and (×) with 8-HQ + BTA; electrode rotation rate: 500 rpm.

Fig. 4. SEM micrographs of AA2024 surface after 20 h of immersion in a 0.1 M Na$_2$SO$_4$ + 0.05 M NaCl solution containing: (a) and (b) BTA, (c) and (d) 8-HQ and (e) and (f) 8-HQ + BTA; electrode rotation rate: 500 rpm.

whereas in the presence of the 8-HQ + BTA mixture, galvanic corrosion was strongly reduced.

3.2. Impedance measurements

Global and local electrochemical impedance measurements were performed to elucidate the role of each inhibitor on the corrosion behaviour of AA2024. Global impedance diagrams were first obtained on pure Al with and without 8-HQ to separate the contribution of the molecule from the impedance response obtained on AA2024. Then, the diagrams were obtained on AA2024 in the presence of 8-HQ or 8-HQ + BTA.

3.2.1. Global impedance measurements

The impedance diagrams obtained on pure aluminium after 20 h of immersion in the neutral solution with and without 8-HQ are shown in Fig. 5 in Bode coordinates. In the absence of inhibitor, the diagram presents only one time constant which is associated to the response of the passive film and to oxygen reduction on the passive layer [39]. In the presence of 8-HQ, the impedance modulus was little modified by comparison with the blank solution whereas two time constants are visible on the phase angle. The first time constant in the high frequency range was attributed to the formation of a protective layer composed of insoluble aluminium chelates [23] while the low frequency part of the diagram characterizes the aluminium oxide layer and oxygen reduction [14]. In the absence of inhibitor, an equivalent circuit composed of a R_{BF}//CPE$_{ox}$ element can be proposed to describe the behaviour of pure Al in the electrolyte (Fig. 6a). The R_{BF} resistance was added to account for the oxygen reduction reaction on the oxide layer. In the solution containing 8-HQ, in order to take into account the presence of the

two time constants, an additional R_f//CPE$_f$ circuit was introduced (Fig. 6b). The two parts of the circuit were imbricated to follow the hypothesis that the presence of the aluminium chelates decreases the active surface in contact with the electrolyte. This equivalent circuit is similar to that often used to describe the behaviour of organic coatings [40,41]. The two circuits (Fig. 6) were chosen to combine the typical features of the impedance diagrams obtained with and without inhibitor and to account for: (i) the presence of the oxide film (anodic reaction); (ii) the film formed with the 8-HQ and (iii) the oxygen reduction reaction (cathodic reaction). Parameters α and Q, introduced into the equivalent circuits, are associated
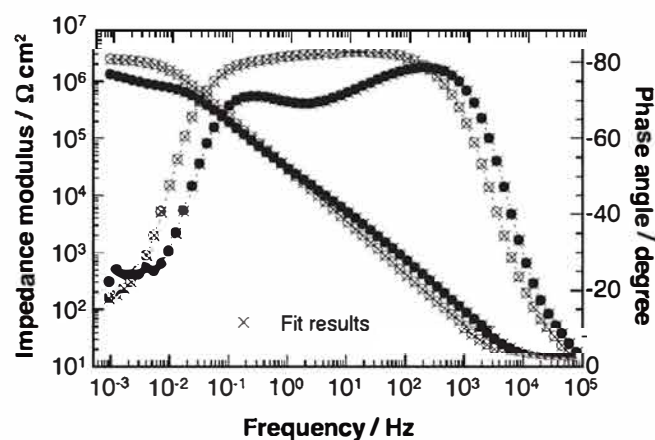

Fig. 5. Electrochemical impedance diagrams obtained on pure aluminium after 20 h of immersion at E_{corr} in a 0.1 M Na$_2$SO$_4$ + 0.05 M NaCl solution: (○) without inhibitor and (●) with 8-HQ; electrode rotation rate: 500 rpm.

Table 3
Fitted parameters obtained for pure aluminium after 20 h of immersion in 0.1 M Na$_2$SO$_4$ + 0.05 M NaCl solutions with or without 8-HQ.

	α_f ± 0.3%	Q_f (Ω^{-1} cm^{-2} s$^\alpha$) ± 2%	R_f (Ω cm^2) ± 7%	(α_{ox}) ± 1%	Q_{ox} (Ω^{-1} cm^{-2} s$^\alpha$) ± 2%	R_{BF} (Ω cm^2) ± 3%
Without inhibitor	–	–	–	0.92	6.2 10^{-6}	2.6 10^6
With 8-HQ (3 × 10^{-3} M)	0.92	3.4 10^{-6}	16 10^3	0.81	3.7 10^{-6}	1.1 10^6

to a constant phase element (CPE). They may result from the distribution of the properties through the film [39,42]. The experimental diagrams with and without 8-HQ are perfectly fitted by the equivalent circuits, as shown in Fig. 5 and the values of the parameters are reported in Table 3. The value of R_f is relatively high (16 kΩ cm^2) indicating the formation of a dense organic film on the pure Al surface. Garrigues et al. have shown that 8-HQ is first adsorbed on the Al surface preventing the adsorption of chloride ions and the improvement of the corrosion resistance with increasing immersion time was attributed to the slow formation of an aluminium chelate [23]. The value of Q_{ox} is lower in the presence of 8-HQ which tends to indicate that the oxide film is thinner in this case. The low values of Q_f and Q_{ox} are indicative of the formation of thin films, either for the alumina film or for the dense layer of aluminium chelate. The value of R_{BF} (Table 3) is lower in the presence of 8-HQ. From the Q_{ox} value, it was assumed that the aluminium oxide film thickness was thinner than that formed without 8-HQ due to the presence of the aluminium chelate which impeded the formation of the aluminium oxide. This hypothesis agreed with the polarisation curves obtained on pure aluminium with and without 8-HQ (not shown in the present manuscript). With 8-HQ, the cathodic current densities were higher than that observed without inhibitor, which can explain the lower impedance value (Fig. 5). However, in the presence of 8-HQ, the formation of the aluminium chelate prevented the dissolution of the aluminium which led to lower anodic current densities. Thus, in the presence of 8-HQ, the increase of the cathodic currents and the decrease of the anodic ones, by comparison with the curves obtained without 8-HQ, explained that, at the corrosion potential, the impedance modulus are close (Fig. 5).

Fig. 7 presents the impedance spectra obtained on AA2024 in the solution containing 8-HQ and in the solution containing 8-HQ + BTA. The diagrams have the same shape as those obtained on pure Al in the solution containing 8-HQ with the presence of two time constants (Fig. 5). It can be observed that the high frequency part of the diagrams is superimposed for the two media whereas the impedance modulus in the low frequency range increased by a factor of ten when the BTA was added to the electrolytic solution. The diagrams are correctly fitted (Fig. 7) with the equivalent circuit proposed for pure Al in the solution containing 8-HQ (Fig. 6b) and the extracted parameters are reported in Table 4. It can be seen that the values of the parameters associated to the organic film (α_f, Q_f and R_f) are relatively similar for the two solutions and the values are close to those obtained on pure Al with the 8-HQ (Table 3). This result indicates that the HF part of the impedance diagrams
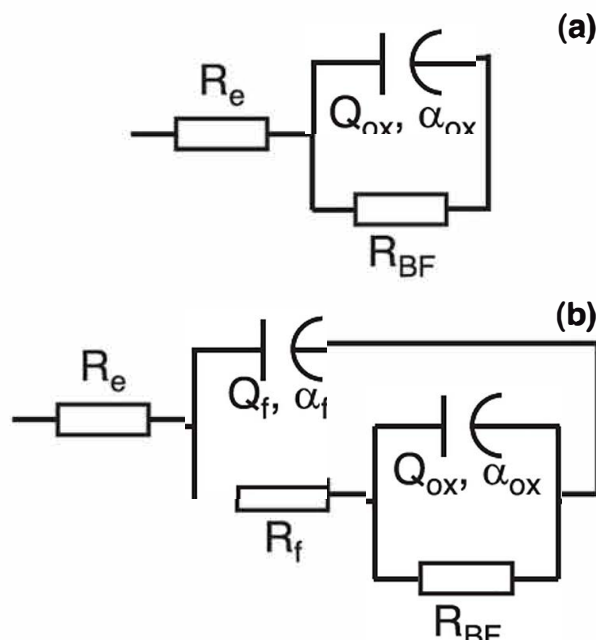
(a)

(b)

Fig. 6. Equivalent electrical circuits used to fit the impedance diagrams for: (a) pure Al in the solution without inhibitor and (b) pure Al and AA2024 in the solution with 8-HQ and 8-HQ + BTA; (R_e: electrolyte resistance; R_f: resistance of the solution in the pores of the organic film; Q_f and α_f: parameters associated to the properties of the organic film; R_{BF}: Resistance associated to the oxygen reduction reaction; Q_{ox} and α_{ox}: parameters associated to the properties of the oxide film).
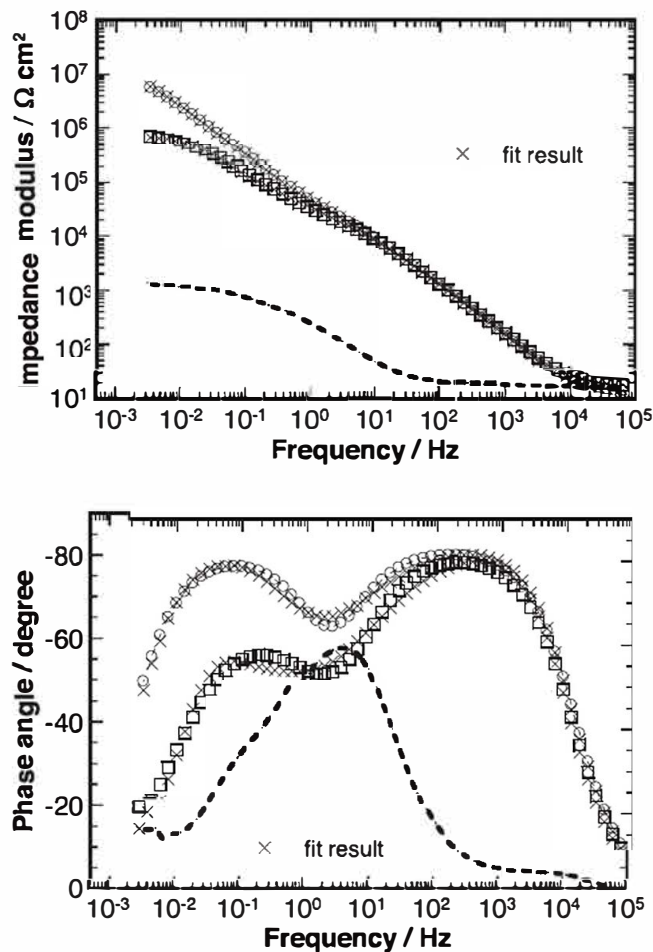
Fig. 7. Electrochemical impedance diagrams obtained on AA2024 after 20 h of immersion at E_{corr} in a 0.1 M Na$_2$SO$_4$ + 0.05 M NaCl solution containing: ($\square$) 8-HQ and ($\bigcirc$) 8-HQ + BTA. The diagram obtained in the absence of inhibitor is reported in dotted line for comparison; electrode rotation rate: 500 rpm.

Table 4
Fitted parameters obtained for AA2024 after 20 h of immersion in 0.1 M Na$_2$SO$_4$ + 0.05 M NaCl solution with 8-HQ and with 8-HQ + BTA mixture.

	$\alpha_f \pm 0.5\%$	$Q_f/(\Omega^{-1}\,cm^{-2}\,s\alpha) \pm 3\%$	$R_f/(\Omega\,cm^2) \pm 5\%$	$\alpha_{ox} \pm 1\%$	$Q_{ox}\,(\Omega^{-1}\,cm^{-2}\,s\alpha) \pm 2\%$	$R_{BF}\,(\Omega\,cm^2) \pm 2\%$
8-HQ (3 × 10^{-3} M)	0.92	2 10^{-6}	25 10^3	0.73	7.1 10^{-6}	10^6
8-HQ (3 × 10^{-3} M) + BTA (10^{-2} M)	0.93	2 10^{-6}	53 10^3	0.91	2.4 10^{-6}	13 10^6

characterizes the action of 8-HQ and it can be concluded that 8-HQ acts mainly on the Al matrix. The parameters associated to the oxide layer and to oxygen reduction (α_{ox}, Q_{ox} and R_{BF}) are modified in the presence of BTA. The significant increase of R_{BF} can be attributed to the specific action of BTA on the Cu-rich intermetallic particles, impeding oxygen reduction. The inhibitive effect leads to a strong limitation of oxygen reduction and thus to an increase of the charge transfer resistance.

For comparison, the impedance diagram obtained in the absence of inhibitor is reported in Fig. 7. At the corrosion potential, the metal is not in the passive state as shown by the polarization curve (Fig. 3). The diagram is characterized by two time constants. The first one (around 1 Hz) is associated to the charge transfer process, mainly on the intermetallic particles, while the second, in the low frequency range, is not clearly defined and is due to the oxygen diffusion, particularly on the intermetallic particles. Comparison of the diagrams clearly shows the inhibitive action of the compounds. The synergistic effect was clearly seen on the impedance results (Fig. 7 and Table 4). R_{BF} is more than ten times higher with the mixture of 8-HQ + BTA than with 8-HQ alone. Moreover, impedance diagrams obtained in the presence of BTA alone, at a concentration of 10^{-2} M (not reported here), showed that R_{BF} was lower than 10^5 Ω cm^2. The synergy can be explained by the two different mechanisms by which BTA and 8-HQ inhibit corrosion of the 2024 aluminium alloy. From the global impedance measurements only an average response of the behaviour of the whole electrode surface was obtained. To identify the role of each inhibitor, particularly on galvanic corrosion at the matrix/intermetallic particles interface, LEIS measurements were performed on an Al/Cu model couple.

3.2.2. Local impedance measurements

Two mappings obtained at 10 Hz above the model couple in the solution without inhibitor and in the presence of the inhibitive mixture are shown in Fig. 8. Without inhibitor (Fig. 8a), admittance is higher (lower resistance) on the copper electrode. This is due to galvanic coupling: oxygen reduction occurs on copper whereas aluminium is in the passive state [34]. In the presence of the inhibitive mixture (Fig. 8b), it can be first noted that the admittance is significantly lower than that obtained without inhibitor, showing the inhibitive efficiency of the compounds. It can be also seen that the admittance is lower on copper (higher resistance) confirming the inhibitive effect of BTA and the limitation of the oxygen reduction reaction on copper.

Local impedance spectra were collected on both electrodes with the radial position of the bi-electrode as a parameter. The local diagrams were obtained in the solution containing BTA, 8-HQ or the inhibitive mixture. They are reported in Nyquist coordinates in Fig. 9a, b and c, respectively. All the diagrams are characterized by inductive loops in the high-frequency range, attributed to local ohmic impedance [38]. In the presence of BTA, capacitive loops with high impedance values are seen on the Cu part indicating the inhibitive action of the molecule. The capacitive behaviour on Al is attributed to the presence of the passive layer on the aluminium surface. In the presence of 8-HQ, the local impedance diagrams on Cu present lower resistance values compared to those obtained with the BTA and conversely on the Al part, the diagrams are characterized by a straight line with no curves, indicating high impedance values. With 8-HQ, the results underline the action of 8-HQ on Al but not specifically on Cu. In the presence of the inhibitive mixture, the local impedance diagrams are characterized by a capacitive behaviour both on Cu and on Al parts and the diagrams are almost superimposed. For each diagram obtained on Al or Cu, in the presence of BTA, 8-HQ and the mixture, the α and Q parameters were graphically extracted [39]. It can be underlined that the values are obtained in a relatively narrow frequency range and the accuracy on their determination is about 10%. Fig. 10 shows the variation of these parameters versus the radial position of the electrode.

In the presence of BTA (Fig. 10a) or in the presence of 8-HQ (Fig. 10b), the Al/Cu interface is clearly visible whereas it is less marked in the presence of the inhibitive mixture (Fig. 10c). In Fig. 10c, it can be seen that the presence of the two inhibitors "equalizes" the α and Q parameters on both sides (Cu and Al). This result can be analysed by comparison with Fig. 10a and b: the α and Q parameters obtained on Cu in the presence of BTA or BTA + 8-HQ are close. Similarly, the α and Q parameters obtained on Al in the presence of 8-HQ or BTA + 8-HQ are comparable. For example, the α values are around 0.7 on Cu with BTA alone (Fig. 10a) and the same values are found on Cu in the presence of 8-HQ + BTA (Fig. 10c). On the other hand, the α values are around 0.7 on Al with 8-HQ alone
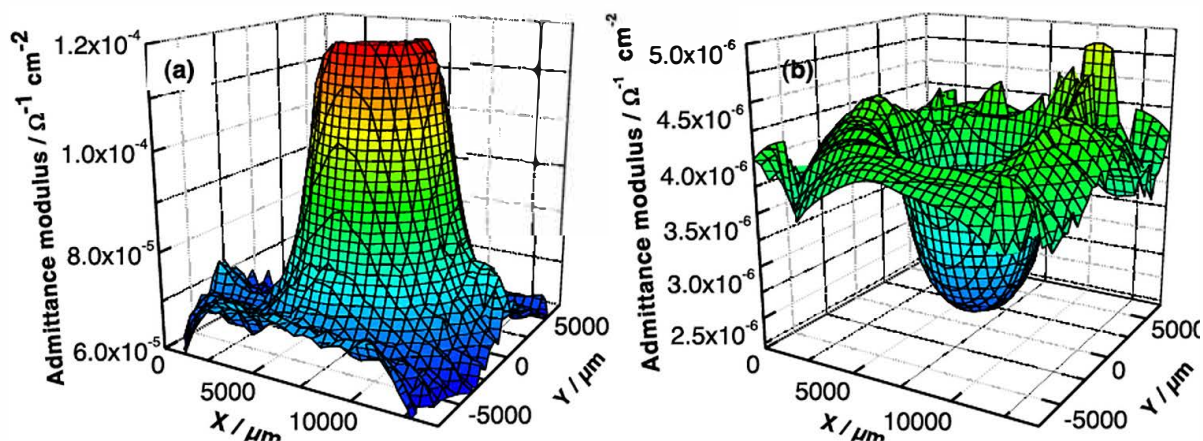

Fig. 8. Mappings obtained at 10 Hz above the Al/Cu couple: (a) after 2 h of immersion in a 10^{-3} M NaCl solution and (b) after 20 h of immersion in deionised water (without NaCl) containing 8-HQ + BTA; static electrode.
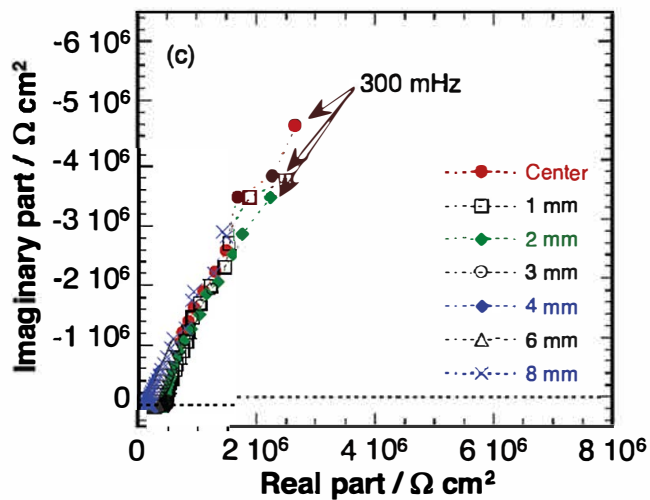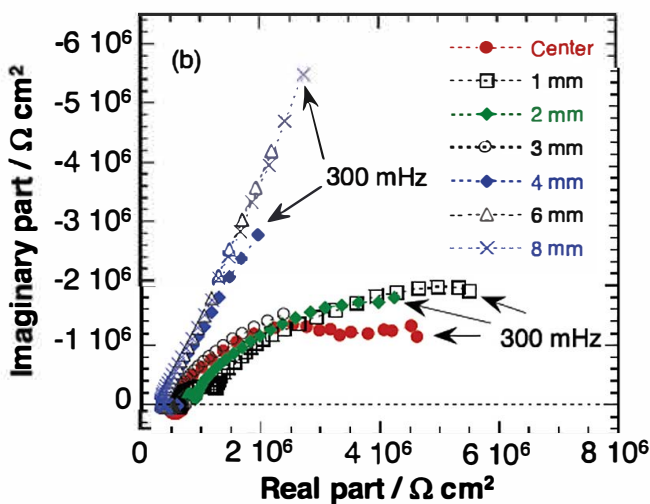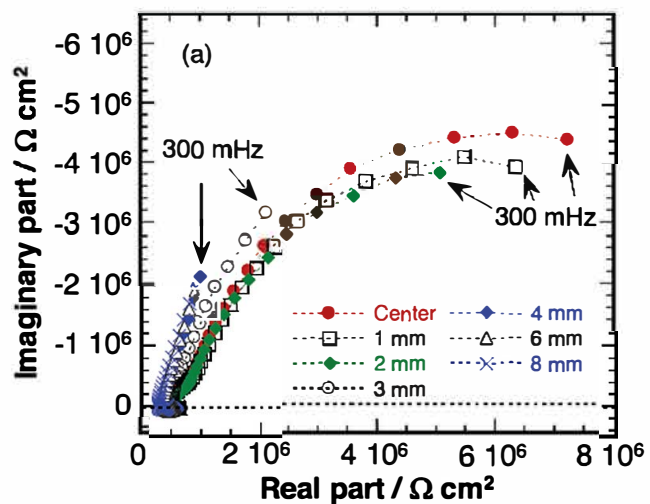
Fig. 9. Local impedance spectra obtained for different radial positions above the Al/Cu couple after 20 h of immersion in aqueous solution (deionised water without NaCl): (a) with BTA, (b) with 8-HQ and (c) with 8-HQ + BTA; static electrode.
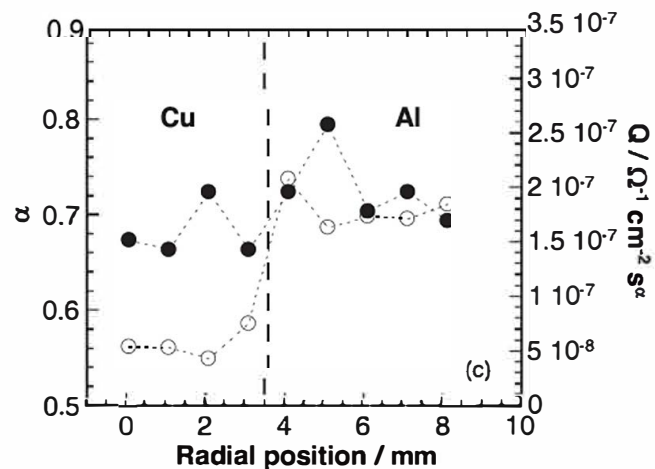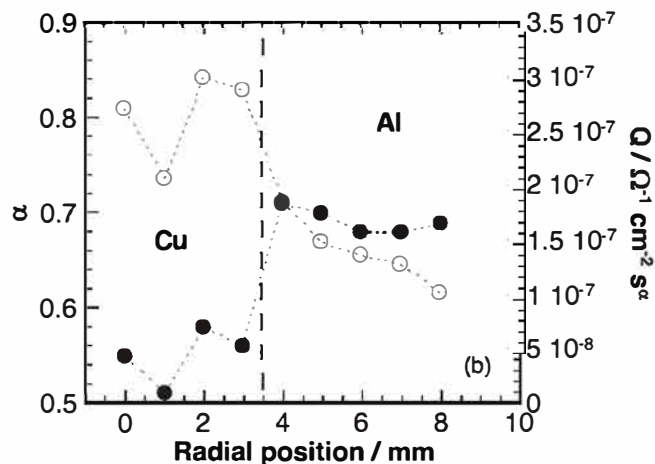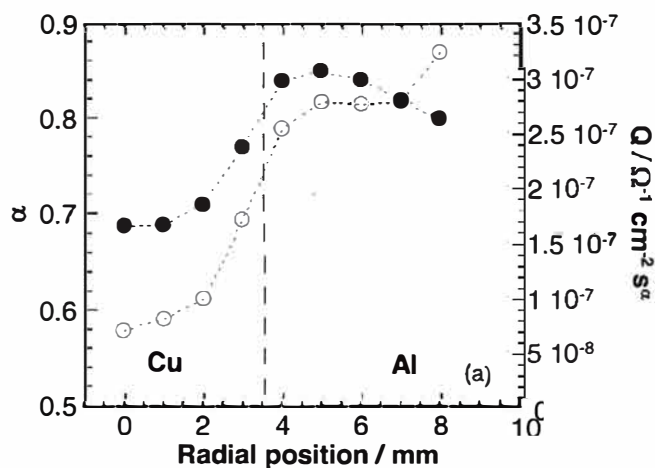
Fig. 10. (●) α and (○) Q parameters obtained from the local impedance spectra for different radial positions above the Al/Cu couple after 20 h of immersion in aqueous solution (deionised water without NaCl): (a) with BTA, (b) with 8-HQ and (c) with 8-HQ + BTA.

(Fig. 10b) and with the mixture (Fig. 10c). This observation supports the hypothesis that 8-HQ acts only on Al and BTA acts only on Cu. Thus, the action of BTA on Cu complemented the action of 8-HQ on Al. To have a better analysis of the α and Q parameters and a better knowledge of the films formed on Cu and Al with BTA, with 8-HQ or with the mixture, additional global and local measurements should be performed on pure Cu and pure Al.

Table 5
Corrosion potential values measured after 20 h of immersion.

	E_{corr}/V vs SCE (deionised water)			E_{corr}/V vs SCE (0.1 M Na_2SO_4 + 0.05 M NaCl)
	Cu	Al	Al/Cu couple	AA2024
8-HQ (3×10^{-3} M)	−0.05	−0.76	−0.47	−0.54
BTA (10^{-2} M)	0.09	−0.93	−0.64	−0.59
8-HQ (3×10^{-3} M) + BTA (10^{-2} M)	−0.05	−0.84	−0.81	−0.67

The Al/Cu interface was observed by optical microscopy after 20 h of immersion in the solution containing the inhibitors (Fig. 11). In the presence of BTA, a deep crevice was formed at the Al/Cu interface. In the presence of 8-HQ, the crevice was still visible and the copper surface presented a bright colour near the interface while, except in this zone, it appeared tarnished. With the inhibitive mixture, the crevice is no longer observed and the two parts of the model couple appear bright. The micrograph clearly shows that in the presence of 8-HQ + BTA the galvanic coupling between Al and Cu disappeared. This is in agreement with the SEM micrographs
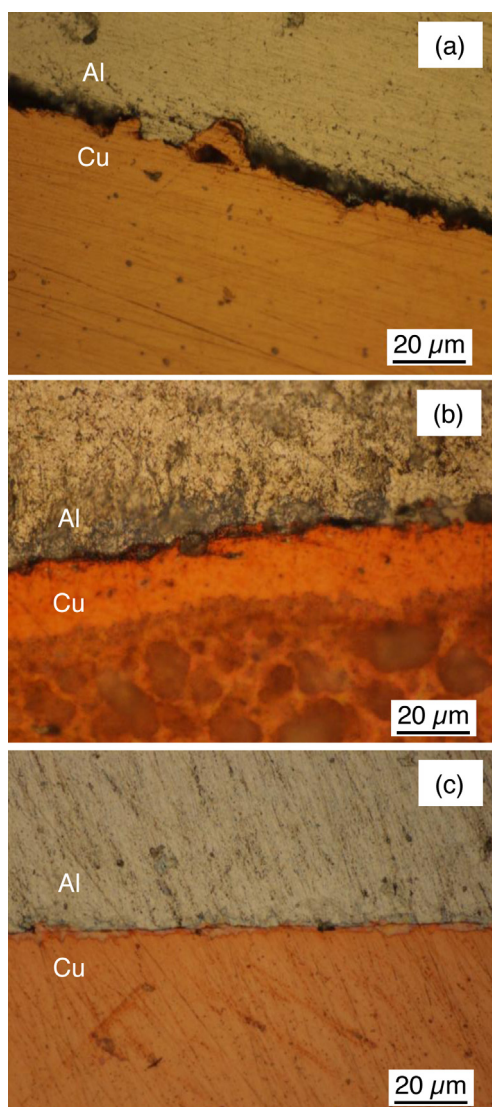

Fig. 11. Optical micrographs of the Al/Cu couple interface after 20 h of immersion in an aqueous solution (deionised water without NaCl): (a) with BTA, (b) with 8-HQ and (c) with 8-HQ + BTA; static electrode.

shown in Fig. 3(f) for the alloy. For AA2024, even though the scale was not the same (4% of copper-rich intermetallic particles instead of 11% copper in the model couple), it can be assumed that the mechanisms are similar [34].

The galvanic corrosion is due to the fact that the corrosion potentials of the two metals in the model couple are different (for the AA2024 the corrosion potential of the Al matrix is different from that of the intermetallic particles). Thus, to have a better insight into the modification of the corrosion potentials in the presence of the inhibitors, the corrosion potentials of pure Al and pure Cu in the presence of 8-HQ, of BTA and of the mixture were measured and compared to that of the Al/Cu model couple. The results are reported in Table 5. It can be seen that for pure Cu, E_{corr} is shifted in the anodic direction in the presence of BTA. For pure Al, E_{corr} is relatively similar with and without BTA, which agrees with the fact that 8-HQ acts only on Al. For the model couple, it is interesting to note that E_{corr} is significantly shifted in the cathodic direction in the presence of the inhibitive mixture and its value is close to that of pure Al in the solution containing the two inhibitors. This result demonstrates that in the presence of the 8-HQ + BTA, the role of Cu becomes negligible due to the high efficiency of BTA which strongly limits oxygen reduction, and as a consequence the galvanic coupling disappears. In the presence of BTA or 8-HQ alone, the corrosion potentials of Cu and Al are different and galvanic coupling cannot be avoided as it observed in the micrographs (Fig. 11). Finally, for comparison, the corrosion potential of the AA2024 is reported in Table 5. Although the E_{corr} values are different from those measured for the model couple (mainly due to the fact that the ratio Cu surface area/Al surface area was different in the model couple and for the alloy), a similar shift of E_{corr} can be observed in the presence of the 8-HQ + BTA mixture by comparison with the E_{corr} values measured in the presence of the compounds tested alone. Thus, in agreement with the other presented results, it can be assumed that the mechanisms are similar for the Al/Cu couple and for the AA2024 in the presence of the inhibitors.

4. Conclusions

The present study confirmed that 8-HQ and BTA are two effective corrosion inhibitors of AA2024. From both global and local electrochemical measurements, it was shown that the mixture of 8-HQ and BTA presented a synergistic effect for the corrosion protection of this alloy. It is explained by the two different mechanisms by which BTA and 8-HQ inhibit corrosion: the action of BTA is mainly limited to the copper-rich intermetallic particles; 8-HQ acts on the aluminium matrix due to its chelating properties. The more significant result is that, in the presence of both compounds, the galvanic coupling responsible for the corrosion process is strongly limited which is not the case when the inhibitors are used separately. This electrochemical result was confirmed by SEM observations.

References

[1] B.R.W. Hinton, N.E. Ryan, D. Arnott, P. Trathen, L. Wilson, B. Williams, The inhibition of aluminum alloy corrosion by rare earth metal cations, Corros. Australas. 10 (1985) 12.

[2] D.R. Arnott, B.R.W. Hinton, N.E. Ryan, Cationic-film-forming inhibitors for the protection of the AA7075 aluminum alloy against corrosion in aqueous solution, Corrosion 45 (1989) 12.

[3] F. Mansfeld, S. Lin, S. Kim, H. Shih, Corrosion protection of Al alloys and Al-based metal matrix composites by chemical passivation, Corrosion 45 (1989) 615.

[4] A.J. Davenport, H.S. Isaacs, M.W. Kendig, XANES investigation of the role of cerium compounds as corrosion inhibitors for aluminium, Corros. Sci. 32 (1991) 653.

[5] A.J. Aldykiewicz, H.S. Isaacs, A.J. Davenport, The investigation of cerium as cathodic inhibitor for aluminum–copper alloys, J. Electrochem. Soc. 142 (1995) 3342.

[6] M. Bethencourt, F.J. Botana, J.J. Calvino, M. Marcos, M.A. Rodriguez-Chacon, Lanthanide compounds as environmentally-friendly corrosion inhibitors of aluminum alloys: a review, Corros. Sci. 40 (1998) 1803.

[7] K.A. Yasakau, M.L. Zheludkevich, S.V. Lamaka, M.G.S. Ferreira, Mechanism of corrosion inhibition of AA2024 by rare-earth compounds, J. Phys. Chem. B 110 (2006) 5515.

[8] N.C. Rosero-Navarro, M. Curioni, R. Bingham, A. Duran, M. Aparicio, R.A. Cottis, G.E. Thompson, Electrochemical techniques for practical evaluation of corrosion inhibitor effectiveness. Performance of cerium nitrate as corrosion inhibitor for AA2024T3 alloy, Corros. Sci. 52 (2010) 3356.

[9] L. Paussa, F. Andreatta, D. De Felicis, E. Bemporad, L. Fedrizzi, Investigation of AA2024-T3 surfaces modified by cerium compounds: a localized approach, Corros. Sci. 78 (2014) 215.

[10] C. Casenave, N. Pébère, F. Dabosi, An electrochemical impedance study of the corrosion inhibition of a 2024 aluminum alloy in neutral chloride solutions, Mater. Sci. Forum 192–194 (1995) 599.

[11] M.L. Zheludkevich, K.A. Yasakau, S.K. Poznyak, M.G.S. Ferreira, Triazole and thiazole derivatives as corrosion inhibitors for AA2024 aluminium alloy, Corros. Sci. 47 (2005) 3368.

[12] S.V. Lamaka, M.L. Zheludkevich, K.A. Yasakau, M.F. Montemor, M.G.S. Ferreira, High effective organic corrosion inhibitors for 2024 aluminium alloy, Electrochim. Acta 52 (2007) 7231.

[13] W. Qafsaoui, F. Huet, H. Takenouti, Analysis of the inhibitive effect of BTAH on localized corrosion of Al 2024 from electrochemical noise measurements, J. Electrochem. Soc. 156 (2009) C67.

[14] G. Boisier, N. Portail, N. Pébère, Corrosion inhibition of 2024 aluminium alloy by sodium decanoate, Electrochim. Acta 55 (2010) 6182.

[15] G. Williams, J.J. Coleman, H.N. McMurray, Inhibition of aluminium alloy AA2024-T3 pitting corrosion by copper complexing compounds, Electrochim. Acta 55 (2010) 5947.

[16] W. Qafsaoui, M.W. Kendig, H. Perrot, H. Takenouti, Coupling of electrochemical techniques to study copper corrosion inhibition in 0.5 mol L^{-1} NaCl by 1-pyrrolidine dithiocarbamate, Electrochim. Acta 87 (2013) 348.

[17] M. Forsyth, T. Markley, D. Ho, G.B. Deacon, P. Junk, B. Hinton, A. Hughes, Inhibition of corrosion on AA2024-T3 by new experimentally friendly rare earth organophosphate compounds, Corrosion 64 (2008) 191.

[18] D. Ho, N. Brack, J. Scully, T. Markley, M. Forsyth, B. Hinton, Cerium dibutylphosphate as a corrosion inhibitor for AA2024-T3 aluminum alloys, J. Electrochem. Soc. 153 (2006) B392.

[19] S.J. Garcia, T.A. Markley, J.M.C. Mol, A.E. Hughes, Unravelling the corrosion inhibition mechanisms of bi-functional inhibitors by EIS and SEM-EDS, Corros. Sci. 69 (2013) 346.

[20] R. Catubig, A. Hughes, I.S. Cole, B.R.W. Hinton, M. Forsyth, The use of cerium and praseodymium mercaptoacetate as thiol-containing inhibitors for AA2024-T3, Corros. Sci. 81 (2014) 45.

[21] K.A. Yasakau, M.L. Zheludkevich, O.V. Karavai, M.G.S. Ferreira, Influence of inhibitor addition on the corrosion protection performance of sol–gel coatings on AA2024, Prog. Org. Coat. 63 (2008) 352.

[22] I.A. Kartsonakis, E. Athanasopoulou, D. Snihirova, B. Martins, M.A. Koklioti, M.F. Montemor, G. Kordas, C.A. Charitidis, Multifunctional epoxy coatings combining a mixture of trapes and inhibitor loaded nanocontainers for corrosion protection of AA2024-T3, Corros. Sci. 85 (2014) 147.

[23] L. Garrigues, N. Pébère, F. Dabosi, An investigation of the corrosion inhibition of pure aluminum in neutral and acid chloride solutions, Electrochim. Acta 41 (1996) 1209.

[24] G.P. Cicileo, B.M. Rosales, F.E. Varela, J.R. Vilche, Inhibitory action of 8-hydroxyquinoline on the copper corrosion process, Corros. Sci. 40 (1998) 1915.

[25] K. Aramaki, T. Kiuchi, T. Sumiyoshi, H. Nishihara, Surface enhanced Raman scattering and impedance studies on the inhibition of copper corrosion in sulfate solutions by 5-substituted benzotriazoles, Corros. Sci. 32 (1991) 593.

[26] X. Liu, G.S. Frankel, B. Zoofan, S. Rokhlin, In-situ observation of intergranular stress corrosion cracking in AA2024-T3 under constant load conditions, Corros. Sci. 49 (2007) 139.

[27] I.L. Muller, J.R. Galvele, Pitting potential of high purity binary aluminium alloys—I. Al–Cu alloys. Pitting and intergranular corrosion, Corros. Sci. 17 (1977) 179.

[28] V. Guillaumin, G. Mankowski, Localized corrosion of 2024 T351 aluminium alloy in chloride media, Corros. Sci. 41 (1998) 421.

[29] W. Zhang, G.S. Frankel, Transitions between pitting and intergranular corrosion in AA2024, Electrochim. Acta 48 (2003) 1193.

[30] C. Blanc, S. Gastaud, G. Mankowski, Mechanistic studies of the corrosion of 2024 aluminium alloy in nitrate solutions, J. Electrochem. Soc. 150 (2003) B396.

[31] P. Schmutz, G.S. Frankel, Corrosion study of AA2024-T3 by scanning Kelvin probe force microscopy and in situ atomic force microscopy scratching, J. Electrochem. Soc. 145 (1998) 2295.

[32] R.G. Buchheit, M.A. Martinez, L.P. Montes, Evidence for Cu ion formation by dissolution and dealloying the Al$_2$CuMg intermetallic compound in rotating ring-disk collection experiments, J. Electrochem. Soc. 147 (2000) 119.

[33] N. Birbilis, R.G. Buchheit, Electrochemical characteristics of intermetallic phases in aluminum alloys: an experimental survey and discussion, J. Electrochem. Soc. 152 (2005) B140.

[34] J.-B. Jorcin, C. Blanc, N. Pébère, B. Tribollet, V. Vivier, Galvanic coupling between pure copper and pure aluminum: experimental approach and mathematical model, J. Electrochem. Soc. 155 (2008) C46.

[35] J.-B. Jorcin, E. Aragon, C. Merlatti, N. Pébère, Delaminated areas beneath organic coating: a local electrochemical impedance approach, Corros. Sci. 48 (2006) 1779.

[36] I. Frateur, V.M.-W. Huang, M.E. Orazem, N. Pébère, B. Tribollet, V. Vivier, Local electrochemical impedance spectroscopy: considerations about the cell geometry, Electrochim. Acta 53 (2008) 7386.

[37] V.M.-W. Huang, S.-L. Wu, M.E. Orazem, N. Pébère, B. Tribollet, V. Vivier, Local electrochemical impedance spectroscopy: a review and some recent developments, Electrochim. Acta 56 (2011) 8048.

[38] C. Blanc, M.E. Orazem, N. Pébère, B. Tribollet, V. Vivier, S. Wu, The origin of the complex character of the ohmic impedance, Electrochim. Acta 55 (2010) 6313.

[39] J.-B. Jorcin, M.E. Orazem, N. Pébère, B. Tribollet, CPE analysis by local impedance spectroscopy, Electrochim. Acta 51 (2006) 1473.

[40] L. Beaunier, I. Epelboin, J.C. Lestrade, H. Takenouti, Etude électrochimique, et par microscopie électronique à balayage, du fer recouvert de peinture, Surf. Technol. 4 (1976) 237.

[41] K. Bonnel, C. Le Pen, N. Pébère, E.I.S. characterization of protective coating on aluminium alloys, Electrochim. Acta 44 (1999) 4259.

[42] M.E. Orazem, I. Frateur, B. Tribollet, V. Vivier, S. Marcelin, N. Pébère, A.L. Bunge, E.A. White, M. Musiani, Dielectric properties of materials showing Contant-Phase-Element (CPE) impedance response, J. Electrochem. Soc. 160 (2013) C215.